Rapid Communications

Cooperative Ru(4*d*)-Ho(4*f*) magnetic ordering and phase coexistence in the 6*H* perovskite multiferroic $Ba_3HoRu_2O_9$

T. Basu [1,2,*] V. Caignaert,[2,†] F. Damay,[3] T. W. Heitmann,[4] B. Raveau,[2] and X. Ke[1,‡]

[1]*Department of Physics and Astronomy, Michigan State University, East Lansing, Michigan 48824, USA*

[2]*Normandie Université, ENSICAEN, UNICAEN, CNRS, CRISMAT, 14000 Caen, France*

[3]*Laboratoire Léon Brillouin, Grenoble, France*

[4]*Missouri Research Reactor, University of Missouri, Columbia, Missouri 65211, USA*

(Received 18 May 2020; revised 5 July 2020; accepted 8 July 2020; published 23 July 2020)

We report cooperative magnetic orderings in a 6*H*-perovskite multiferroic system, $Ba_3HoRu_2O_9$, via comprehensive neutron powder diffraction measurements. This system undergoes long-range antiferromagnetic ordering at $T_{N1} \sim 50$ K with a propagation wave vector of $K_1 = (0.5\,0\,0)$, a transition temperature much higher than the previously reported one at ~10 K (T_{N2}). Both Ru and Ho moments order simultaneously below T_{N1}, followed by spin reorientations at lower temperatures, demonstrating strong Ru(4*d*)-Ho(4*f*) magnetic correlation. Below T_{N1} another magnetic phase with a propagation wave vector $K_2 = (0.25\,0.25\,0)$ emerges and coexists with the one associated with K_1, which is rarely observed and suggests complex magnetism due to phase competition in the magnetic ground state. We argue that the exchange striction arising from the up-up-down-down spin structure associated with a K_2-wave vector below T_{N2} may be responsible for the small ferroelectric polarization reported previously in this compound.

DOI: 10.1103/PhysRevB.102.020409

The electronic and magnetic correlation of *d* and *f* electrons has been a core research topic in condensed-matter physics, and it plays a decisive role in determining material properties such as unconventional superconductivity, metal-insulator transition, magnetoresistance, multiferroicity, as well as a rich variety of magnetic orderings. In particular, the strong *d*-*f* magnetic correlations with competing magnetic interactions often give further interesting properties. For instance, the compounds containing magnetic rare-earth (*R*) ions and transition-metal (TM) ions, e.g., $RMnO_3$ [1], RMn_2O_5 [1–3], and R_2BaNiO_5 [4,5], undergo simultaneous ordering of TM and *R*-moments due to 3*d*-4*f* magnetic correlation, exhibiting intriguing multiferroicity/strong magnetoelectric coupling.

While there have been extensive studies on materials exhibiting 3*d*-4*f* coupling in recent years, much fewer reports in the literature exist on materials composed of both heavy *R* and 4*d* TM ions that could potentially possess strong 4*d*-4*f* coupling [6,7], specifically considering the fact that 4*d*/5*d* electron orbitals are of special interest due to their compelling effects of large spin-orbit coupling and extended *d*-orbitals. The fascinating pyrochlore ruthenates $R_2Ru_2O_7$ exhibit Ru^{4+} ordering at high temperature followed by the ordering of rare-earth ions at lower temperature induced by the 4*d*-4*f* coupling [8–10]. However, unlike other *R*- members, the magnetic ordering of Er and Ru in $Er_2Ru_2O_7$ is still ambiguous, where the effects of strong magnetic anisotropy and the crystal-field effect are speculated [11,12]. The double perovskites A_2RRuO_6 (A = Sr, Ba) exhibit successive magnetic ordering of Ru^{5+} at high temperature followed by *R*-ordering at lower temperature for R = Ho, Er, whereas simultaneous magnetic ordering is observed for R = Nd and Dy [13–15]. On the other hand, only one magnetic anomaly is reported for the $Ba_4RRu_3O_{12}$ system, where the role of Ru^{4+}/Ru^{5+} and R^{3+} ions remains unclear [16]. Therefore, the *d*-*f* magnetic correlation is always intriguing for different *R*-ions not only for compounds in the same family but also for systems with distinct crystal structures/space groups. Another system of current interest is 6*H*-perovskite $Ba_3BB'_2O_9$ (B = 3*d* transition metal/Sr/Ca/Na/lanthanides, $B' = 4d/5d$ metal like Ru, Nb, Sb, Ir), which exhibits versatile exotic properties depending on the nature of B and B' ions, such as a dimer system, geometrical frustration, quantum spin-liquid, charge-ordering, unusual valence state, multiferroicity, etc. [17–26].

The system $Ba_3RRu_2O_9$, crystallizing in 6*H*-perovskite structure, consists of Ru_2O_9 dimers (face-sharing RuO_6 octahedra) that are interconnected by corner-sharing MO_6 octahedra and possess an average valence state of 4.5 of an Ru ion when $R = R^{3+}$. Recently, we have reported magnetodielectric (MD) coupling for $Ba_3RRu_2O_9$, which is significantly enhanced for the heavier rare-earth member $Ba_3HoRu_2O_9$ [25,27]. Such an enhanced MD coupling and the emergent ferroelectricity in $Ba_3HoRu_2O_9$ were speculated to arise from stronger 4*d*-4*f* magnetic correlation between Ru and heavy *R*-ions [25]. The light rare-earth compound $Ba_3NdRu_2O_9$ exhibits a ferromagnetic ordering of Nd moments at $T_c \sim 24$ K, followed by an antiferromagnetic (AFM) ordering of an Ru_2O_9 dimer ~18 K and canted AFM ordering of Nd ~ 17 K [20,28]. In contrast, the heavy–rare-earth members (R = Tb,

*tathamaybasu@gmail.com

†vincent.caignaert@ensicaen.fr

‡kexiangl@msu.edu

Gd, Ho, Er, etc.) undergo AFM ordering at low temperature ~10 K, which is ascribed to the ordering of rare-earth ions, without any further magnetic ordering down to 2 K [29]. Up to now, there has been no report of a detailed magnetic structure of this $Ba_3RRu_2O_9$ system for any heavy–rare-earth member in this series, which is warranted in order to confirm the speculation of strong $4d$-$4f$ magnetic correlation for heavy R-members.

In this paper, via comprehensive neutron powder diffraction measurements, we report simultaneous magnetic ordering of Ru^{4+}/Ru^{5+} and Ho^{+3} moments in $Ba_3HoRu_2O_9$ at $T_{N1} \sim 50$ K, which is ascribed to strong $4d$-$4f$ magnetic correlation. A rare phase coexistence of two different magnetic structures with $\mathbf{K_1} = (0.5\,0\,0)$ and $\mathbf{K}_2 = (0.25\,0.25\,0)$ is revealed below $T_{N2} \sim 10$ K, arising from competing exchange interactions. The up-up-down-down spin structure associated with K_2 is likely intimated with the ferroelectricity below T_{N2} of this compound.

High-quality $Ba_3HoRu_2O_9$ polycrystalline samples were synthesized using the solid-state chemistry method as described in our earlier report [25]. Magnetic susceptibility measurements were conducted using the Superconducting Quantum Interference Device (SQUID) magnetometer, and heat capacity measurements were performed using the Physical Properties Measurements System (PPMS), both produced from Quantum Design. Neutron powder diffraction measurements were carried out using a two-axis diffractometer G4.1 with an incident neutron wavelength of 2.425 Å in LLB (Laboratoire Léon Brillouin, France) and a triple-axis spectrometer (TRIAX) with an incident neutron wavelength of 2.359 Å at the University of Missouri Research Reactor. The magnetic structure was resolved using the FULLPROF and SARAH programs [30,31].

The inset of Fig. 1(a) shows the temperature dependence of dc magnetic susceptibility χ measured in the presence of 1 T magnetic field. The drop in χ below 10 K (assigned as T_{N2}) indicates an antiferromagnetic (AFM) phase transition, which agrees well with the previous reports [25,29]. The inverse susceptibility [Fig. S1 in the supplemental material (SM)] [32] deviates from linearity (Curie-Weiss behavior) below ~100 K, implying the presence of magnetic correlation in this system far above T_{N2}. Figure 1(a) presents the specific heat divided by temperature (C/T) in the presence of $H = 0$ and 5 T dc magnetic field as a function of temperature. The C/T is nearly constant down to 50 K from high temperature (see also Fig. S1 in the SM for a broader view) [32], then slowly decreases upon lowering the temperature until around 13 K, followed by a λ-shape anomaly around 10 K [Fig. 1(a)] in the absence of a magnetic field, which confirms the long-range magnetic ordering at T_{N2}. In the presence of 5 T magnetic field, the feature at T_{N2} shifts to lower temperature (~8 K), consistent with the AFM nature of this system. Interestingly, one can see that the curve measured at $H = 0$ and 5 T starts to bifurcate below ~45 K, further suggesting the presence of magnetic correlation at much higher temperature compared to T_{N2}.

To have a better understanding of the magnetic ordering of $Ba_3HoRu_2O_9$, we have performed neutron power diffraction measurements. Figure 1(b) shows the diffraction intensity as a function of momentum transfer Q measured at several

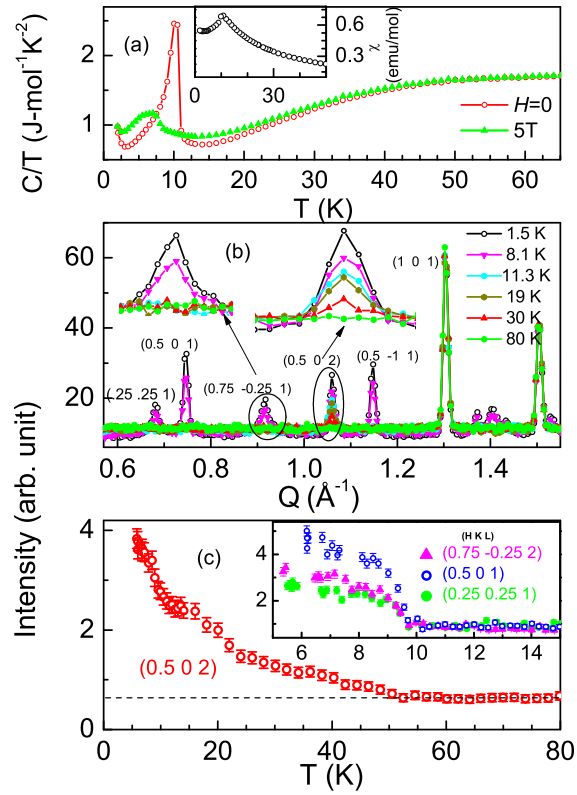

FIG. 1. (a) Heat capacity as a function of temperature measured at $H = 0$ and 5 T. The inset of (a) shows the magnetic susceptibility as a function of temperature measured at $H = 1$ T. (b) Powder neutron diffraction pattern collected at different temperatures from 1.5 to 80 K in the low Q-region. Selected magnetic Bragg peaks are indexed, as described in the text, and the insets show the expanded views. (c) Magnetic Bragg peak intensity of (0.5 0 2) plotted as a function of temperature measured at zero field. The inset shows the ordering parameter measurements of (0.75 −0.25 1), (0.5 0 1), and (0.25 0.25 1) magnetic Bragg peaks.

temperatures ranging from 1.5 to 80 K. The insets present an expanded view at $Q = 0.93$ and 1.07 Å^{-1}. There are several important features worth pointing out: (i) There is no change of nuclear Bragg peaks (see also Fig. S2 in the SM) [32] at all temperatures measured, which indicates no structural phase transition down to 1.5 K. (ii) Below T_{N2}, for instance at $T = 8.1$ K and 1.5 K, there are extra peaks showing up at $Q = 1.07$, 0.93, 0.75, and 0.69 Å^{-1} compared to the data measured at $T = 80$ K, indicating their magnetic nature, and as will be discussed next, the wave vectors associated with these Q values are (0.5 0 2), (0.75 −0.25 1), (0.5 0 1), and (0.25 0.25 1), respectively. (iii) Intriguingly, as shown in the inset of Fig. 1(b), the magnetic Bragg peak at $Q = 1.07$ Å^{-1} persists even above T_{N2}, for instance at $T = 11.3$, 19, and 30 K, while magnetic Bragg peaks at other Q values disappear. This suggests the presence of another magnetic ordering between 30 and 80 K, which is far above the previously reported magnetic transition at ~10 K (T_{N2}). To obtain magnetic ordering temperatures, Fig. 1(c) and its inset present the temperature dependence of scattering intensities measured at the aforementioned four Q values. In contrast to other magnetic Bragg peaks whose intensity drops to the

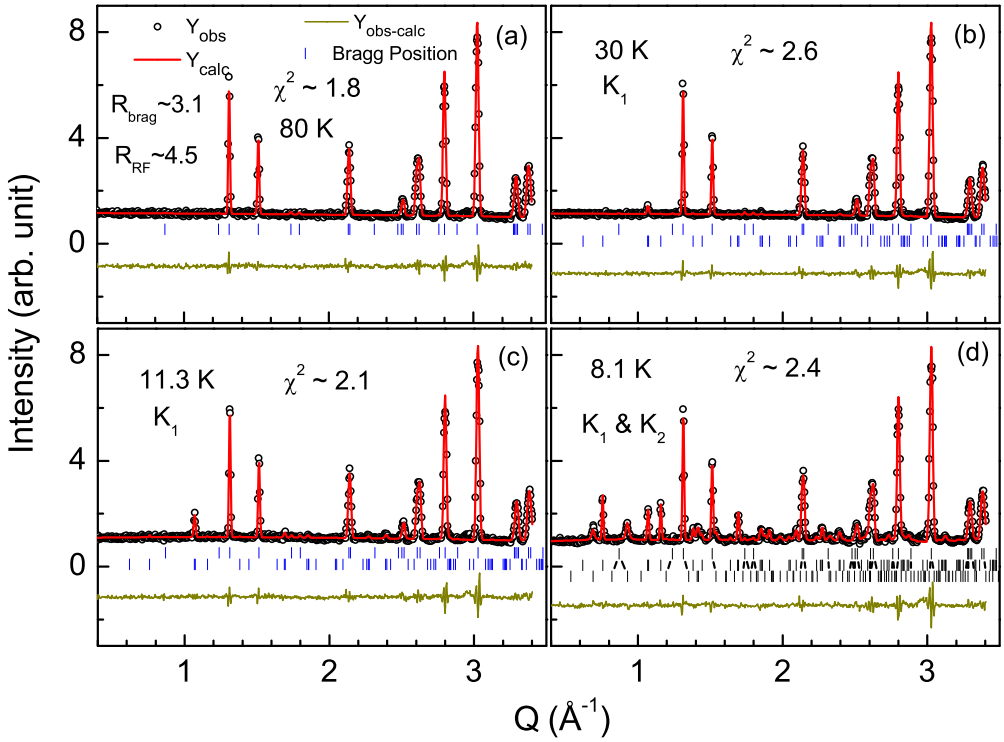

FIG. 2. Powder neutron diffraction pattern collected at $T = 80$ K (a), 30 K (b), 11.3 K (c), and 8.1 K (d) in zero magnetic field. The open black circle represents the experimental data, while the red solid line shows the Rietveld fitting. The vertical bars display the Bragg peak positions. The upper vertical lines represent Bragg peaks of the crystal structure of $Ba_3HoRu_2O_9$, the next lower vertical lines represent magnetic Bragg peaks associated with $\mathbf{K}_1 = (0.5\,0\,0)$ [for (b), (c), and (d)], and the lowest vertical line in (d) represents magnetic Bragg peaks associated with $\mathbf{K}_2 = (0.25\,0.25\,0)$. The continuous dark yellow at the bottom of the figure shows the difference between the experimental and calculated intensity.

background signal at T_{N2}, the Bragg peak intensity of the (0.5 0 2) peak sharply decreases with increasing temperature from 2 K [Fig. 1(c)], and becomes nearly constant around T_{N2}, followed by a gradual drop above 15 K until it reaches the background signal around 50 K (T_{N1}). These features clearly indicate that the system undergoes two magnetic phase transitions, one at $T_{N1} \sim 50$ K and the other at $T_{N2} \sim 10$ K.

Rietveld refinement of the neutron diffraction data measured at several temperatures using the SARAH and FULLPROF programs is presented in Fig. 2. The nuclear scattering data at 80 K [Fig. 2(a)] are well-fitted with the space group $P6_3/mmc$, which affirms the high crystalline quality of the sample. We do not find any impurity via Rietveld refinement within the resolution limit of the instrument (<2%). For magnetic refinement, the possible propagation (**K**) vectors associated with this space group are listed in Table S1 in the SM [32]. We identify the magnetic propagation vector of the neutron diffraction measured at 30 and 11.3 K (i.e., $T_{N1} < T < T_{N2}$) to be $\mathbf{K_1} = (0.5\,0\,0)$. Considering the space group $P6_3/mmc$ and $\mathbf{K_1} = (0.5\,0\,0)$, there are 4-irreducible representations associated with Ho atom, represented by $\Gamma_{\rm mag}(\text{Ho}) = 1\Gamma_1^1 + 0\Gamma_2^1 + 2\Gamma_3^1 + 0\Gamma_4^1 + 1\Gamma_5^1 + \Gamma_6^1 + 2\Gamma_7^1 + 0\Gamma_8^1$, and 8-irreducible representation associated with Ru atom, represented by $\Gamma_{\rm mag}(\text{Ru}) = 1\Gamma_1^1 + 2\Gamma_2^1 + 2\Gamma_3^1 + 1\Gamma_4^1 + 1\Gamma_5^1 + \Gamma_6^1 + 2\Gamma_7^1 + 1\Gamma_8^1$ (see Tables S2 and S3 in SM [32]). As both Ru and Ho atoms have ordered magnetic moments, their irreducible representations should contain any of the combinations of Γ_1, Γ_3, Γ_5, and Γ_7. Among these four representations, the Γ_7 model gives the best fit [Figs. 2(b) and 2(c)]. We found that the magnetic peak profile is best modeled only when both Ho and Ru atoms have nonzero magnetic moment (details are discussed in the SM [32]; see Fig. S2). Below T_{N2} we find that the propagation of the magnetic Bragg peaks can be indexed with propagation vectors of $\mathbf{K_1} = (0.5\,0\,0)$ and $\mathbf{K}_2 = (0.25\,0.25\,0)$, indicating that two different magnetic phases coexist. Figure 2(d) shows the neutron scattering data measured at $T = 8.1$ K and the refinement results. Considering the space group $P6_3/mmc$ and $\mathbf{K}_2 = (0.25\,0.25\,0)$, there are 4-irreducible representations associated with the Ho atom, represented by $\Gamma_{\rm mag}(\text{Ho}) = 1\Gamma_1^1 + 1\Gamma_2^1 + 2\Gamma_3^1 + 2\Gamma_4^1$, and there are 4-irreducible representations associated with the Ru atom, represented by $\Gamma_{\rm mag}(\text{Ru}) = 3\Gamma_1^1 + \Gamma_2^1 + \Gamma_3^1 + 3\Gamma_4^1$ (see Tables S4 and S5 in the SM [32]). We find that a combination of Γ_1 [for $\mathbf{K}_2 = (0.25\,0.25\,0)$] and Γ_7 [for $\mathbf{K_1} = (0.5\,0\,0)$] models gives the best refinement result below T_{N2}. The Rietveld refinement for 1.5 K data is shown in Fig. S4 in the SM [32]. This infers that two different magnetic phases coexist below T_{N2}. The neutron peak shape is modeled with a Thompson-Cox-Hastings pseudo-Voigt function in the FULLPROF program, which is a convolution of Lorentzian and Gaussian functions. The peak shape of the magnetic Bragg reflections associated with the $\mathbf{K}_1$ vector is Gaussian (negligible Lorentzian part), whereas the magnetic Bragg reflections associated with the $\mathbf{K}_2$ vector have a small Lorentzian component along with a Gaussian one, which implies that the magnetic correlation length associated with

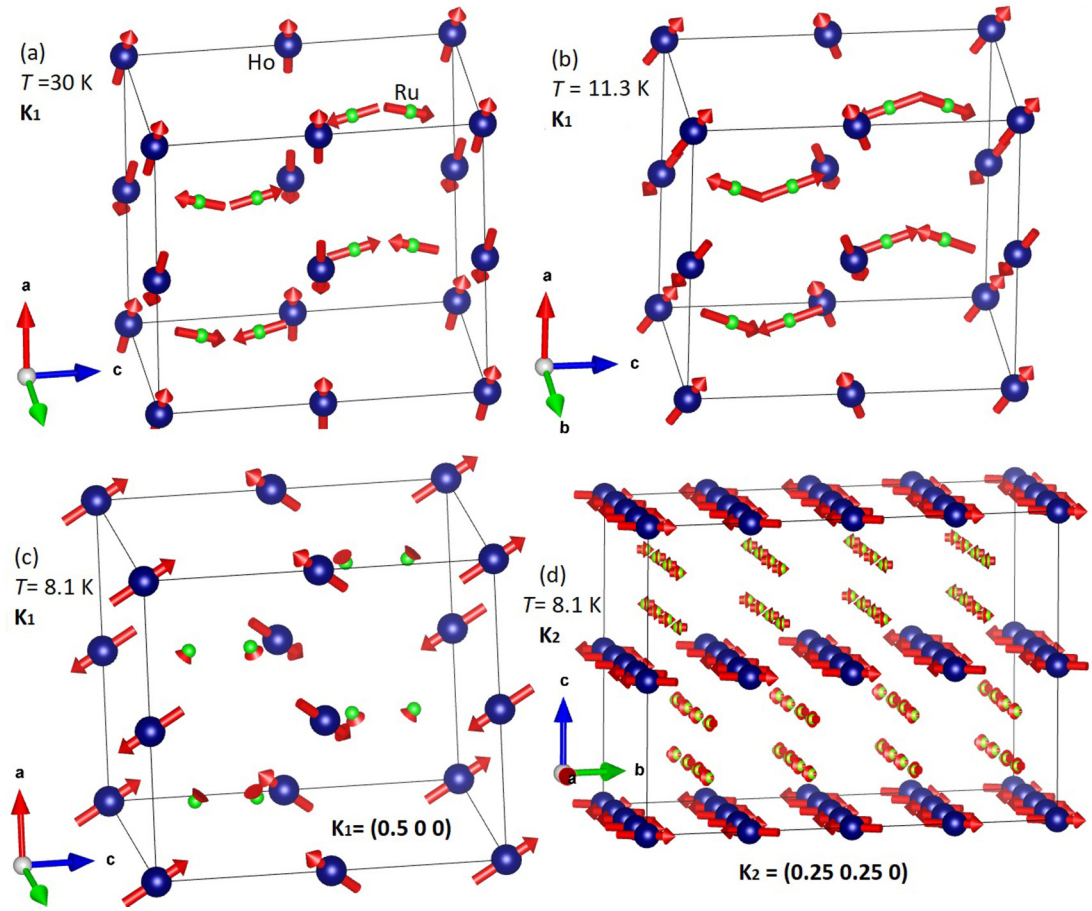

FIG. 3. Parts (a) and (b) represent magnetic structure at $T = 30$ and 11.3 K, respectively. Parts (c) and (d) represent magnetic structure at 8.1 K, associated with $\mathbf{K}_1$ and $\mathbf{K}_2$, respectively. The length of the magnetic vectors represents the relative moment size of Ho (blue) and Ru (green) at that particular temperature.

the $\mathbf{K}_2$ structure is shorter than that associated with the $\mathbf{K}_1$ structure.

The magnetic structures associated with these two magnetic phases are depicted in Fig. 3. At $T_{N2} < T < T_{N1}$, for instance, where $T = 30$ K, both Ho and Ru spins are ordered ferromagnetically along the b axis and antiferromagnetically in the ac plane (AFM along the a axis and canted AFM along the c axis), as shown in Fig. 3(a). The Ho spins are nearly aligned in the ab plane with a slight tilting toward the c axis, whereas the Ru spins are nearly aligned along the c axis with a tilting toward the ab plane. Upon lowering the temperature, the magnetic structure remains nearly the same but with more tilting of both Ho and Ru moments toward the c axis and an enhanced moment size [Fig. 3(b) for 11.3 K and Table I]. This is indicative of strong $4d$-$4f$ magnetic correlation in this system. The slow rotation of Ru and Ho moments is observed upon lowering the temperature. However, the tilting of Ho moments toward the c axis is enhanced negligibly at 11 K compared to that of 19 K, whereas the change in canting angle observed between 19 and 30 K is larger (see Table I). This results in a gradual but anomalous change in the intensity of the (0.5 0 2) magnetic peak [Fig. 1(c)] due to the change in magnetic structure factor in addition to the enhancement of the magnetic moment value. Below T_{N2}, there is a change in magnetic structure. Figures 3(c) and 3(d) represent the magnetic structures associated with $\mathbf{K_1} = (0.5\,0\,0)$ and $\mathbf{K}_2 = (0.25\,0.25\,0)$ propagation wave vectors, respectively, by refining the neutron scattering data measured at $T = 8.1$ K. As illustrated in Fig. 3(c), the magnetic structure associated with $\mathbf{K}_1$ remains nearly the same below and above T_{N2}. Nevertheless, the component of the Ho magnetic moment (M_c) along the c axis is significantly enhanced below T_{N2}, compared to the M_a and M_b components along the a and b axes (see Table I). In contrast, M_c of the Ru-magnetic moment is significantly reduced, compared to the M_a and M_b components, which is distinct from the scenario observed above T_{N2}. Interestingly, such spin reorientation of both Ho and Ru moments gives rise to the extinction of the (0.5 0 1) and (0.5 −1 1) magnetic Bragg peaks above T_{N2} while the (0.5 0 2) magnetic Bragg peak persists. The calculated and experimentally obtained intensities of the magnetic peaks are listed in Table S6 in the SM [32]. Figure 3(d) shows the refined magnetic structure associated with $\mathbf{K}_2$. For this magnetic phase, both Ho and Ru spins are completely aligned in the ab plane with an up-up-down-down antiferromagnetic structure, while spins are ferromagnetically aligned along the c axis. Note that the total magnetic moment of the Ho atom is nearly saturated ($\sim 10.1\,\mu_B$) at $T = 8.1$ K, and the total magnetic moment of Ru is about $1.6\,\mu_B$. The magnetic structure remains the same down to $T = 1.5$ K (Figs. S5 and S6

TABLE I. The magnetic moment of Ru and Ho and its projection along different axis and angle.

	$K_1 = (0.5\,0\,0)$									
	Ho moment (μ_B)				Ru moment (μ_B)				Angle with c-axis (deg)	
T (K)	M_a	M_b	M_c	M_{Ho}	M_a	M_b	M_c	M_{Ru}	M_{Ho}	M_{Ru}
80										
30	1.197	0.599	−0.102	1.042	−0.289	−0.144	0.778	0.817	94.4	22.5
19	1.452	0.726	−0.484	1.347	−0.717	−0.359	1.262	1.406	106.6	32.4
11.3	1.544	0.772	−0.648	1.486	−0.761	−0.380	1.443	1.586	110.6	30.5
8.1	3.447	1.723	3.951	4.952	−0.510	−0.255	0.281	0.524	44.3	116.3
1.5	4.089	2.044	4.665	5.856	−0.489	−0.245	0.388	0.574	44.4	54.6
	$K_2 = (0.25\,0.25\,0) T < T_{N2}$									
8.1	4.127	4.127	0	4.127	1.245	0.865	0	1.105	90	90
1.5	4.920	4.920	0	4.920	1.148	0.531	0	0.995	90	90

in the SM [32]). The smooth increase of the magnetic Bragg peak intensity below T_{N2} [main panel and inset of Fig. 1(c)] is due to the enhancement of the magnetic moments toward saturation. The application of a high magnetic field may flip the spin along H and may transform the up-up-down-down spin structure to the up-up-up-down spin structure. The H-induced magnetic transition with weak hysteresis around ∼3 T in isothermal magnetization (Ref. [25]) could be attributable to a spin-flip transition.

The observation of two magnetic orderings in $Ba_3HoRu_2O_9$ is quite intriguing. First, no clear anomaly at the onset of long-range ordering (LRO) around 50 K (T_{N1}) is observed in either bulk magnetic susceptibility or heat capacity measurements, although the Gaussian nature of the peak shape of magnetic reflections associated with $\mathbf{K}_1$ confirms the LRO below T_{N1}. This is presumably because the magnetic ordering at T_{N1} is weak in nature, where both Ho and Ru spins start to order but with small magnetic moment. Because of short-range magnetic correlation above T_{N1}, entropy starts to vary slowly from high temperature, crosses over with a minimal change around T_{N1} due to weak magnetic ordering, followed by further gradual changes due to continuous slow spin-saturation and spin-reorientation with further lowering temperature. Despite the absence of anomaly in heat capacity at T_{N1}, one can clearly observe the onset of a bifurcation of heat capacity measured at zero and high magnetic field as shown in Fig. 1(a). Right below T_{N2} the Ho moment quickly saturates and there is also a sharp spin-reorientation of Ho and Ru moments, which gives rise to a maximum in the temperature-dependent magnetic susceptibility and a large change in entropy leading to an anomaly in heat capacity. The absence of anomaly in magnetic susceptibility and heat capacity at the onset of magnetic ordering is unusual but not rare. The Haldane spin-chain system (R_2BaNiO_5) exhibits similar features [5], where long-range magnetic ordering develops at high temperature as revealed by neutron diffraction measurement, but it does not yield an anomaly in magnetic susceptibility and heat capacity until spin-reorientation and spin-saturation occur at lower temperature.

Second, Ho and Ru spins simultaneously develop long-range ordering below T_{N1}. In general, rare-earth ions often order at relatively low temperature because of the weak magnetic correlation due to their localized f orbitals. For instance, $Ho_2Ru_2O_7$ undergoes two magnetic phase transitions with Ru moment ordered at higher temperature (∼95 K) followed by the ordering of Ho ions at lower temperature (∼1.4 K) due to the enhanced internal magnetic field arising from the ordered Ru sublattice [8,9]. The concurrent ordering of Ho and Ru moment at 50 K in $Ba_3HoRu_2O_9$ in the current study signals stronger Ho(4f)-Ru(4d) magnetic correlation. Based on Goodenough-Anderson-Kanamori rules, the dominant nearest-neighbor exchange interactions in this system include (i) strong 179° Ru-O-Ho antiferromagnetic superexchange interaction (see the crystal structure in Fig. S6 in SM) [32], (ii) 78° Ru-O-Ho antiferromagnetic superexchange interaction, and (iii) weak Ru-Ru ferromagnetic direct exchange interaction [Ru-Ru of a dimer ∼2.55 Å, which is less than the Ru-Ru distance (2.65 Å) in a metal]. The dominant 179° Ru-O-Ho antiferromagnetic superexchange compared to Ru-O-Ru and Ru-Ru magnetic interaction in $Ba_3Ho^{+3}Ru^{+4.5}{}_2O_9$ could be one possible reason for the simultaneous magnetic ordering of Ru and Ho ions compared to that of the $Ho_2Ru_2O_7$ system (where Ho-O-Ru and Ru-O-Ru both exhibit ∼ 109° superexchange interaction) [9]. The light R-member $Ba_3NdRu_2O_9$ in this family exhibits FM ordering below 24 K, followed by another magnetic ordering ∼17–18 K. The Nd moments align ferromagnetically below 24 K associated with a (0 0 0) wave vector and become canted antiferromagnetically ordered below 17 K with the same K vector, whereas Ru_2O_9 dimers order antiferromagnetically with a (0.5 0 0) wave vector [20], unlike this compound. The Ru moments are non-collinear in a Ru_2O_9 dimer in the tilted system, unlike FM arrangement of Ru moments in intradimer in $Ba_3NdRu_2O_9$ compound [20], and unlike the earlier prediction of AFM dimer in this family for all R-members [17,28,29].

Third, two distinct magnetic phases coexist below T_{N2}, as illustrated in Figs. 3(b) and 3(c). One is associated with $\mathbf{K_1} = (0.5\,0\,0)$ and the other is associated with $\mathbf{K}_2 = (0.25\,0.25\,0)$. Each $\mathbf{K}$ vector corresponds to simultaneous magnetic ordering of both Ru and Ho, unlike many other complex systems where two different $\mathbf{K}$ vectors are associated, with two different magnetic sublattices for different atoms or different crystallographic sites of the same atom [33–35]. Simultaneous ordering of both TM and R ions at

high temperature is also reported in the multiferroic compounds RMn_2O_5 [3,36–38] and R_2BaNiO_5 [4,5], which exhibit successive magnetic anomalies at lower temperature. However, no such magnetic phase coexistence was observed at a particular same T regime for these oxides. Magnetic phase coexistence below metal-insulator transition temperature was observed in a layered ruthenate system, Fe-doped $Ca_3Ru_2O_7$, where the coexistence of commensurate and incommensurate phases arises from competing FM and AFM in-plane Ru-Ru interactions [39]. Note that the incommensurate phase stems from the commensurate one as a result of modification in the FM exchange interaction due to Fe doping. In contrast, here we demonstrate an unconventional magnetic phase coexistence in a magnetically three-dimensional compound, $Ba_3HoRu_2O_9$, where two coexisting magnetic phases are completely different and the phase competition arises as a result of different competing exchange interactions. It is likely that the Ho-O-Ru superexchange interaction starts to dominate below T_{N2}, and Ru moments align with stronger Ho moments, which results in spin-reorientation and the emergence of another spin configuration within the *ab* plane by minimizing the exchange frustration. However, other parameters, such as the crystal-field effect and magnetic anisotropy, may play a role as well, which needs further theoretical/spectroscopic investigations. An external parameter, such as magnetic field or pressure, may stabilize to a particular magnetic phase by tuning the competing interactions.

The Lorentzian part in the peak shape of magnetic reflections associated with $\mathbf{K}_2$ indicates a shorter magnetic correlation length compared to that of an ideal 3D long-range-ordered magnet. However, the λ-shape anomaly in heat capacity below T_{N2} is consistent with LRO as observed in a typical LRO system. It is likely that the system forms finite-size magnetic domains instead of a perfect LRO below T_{N2} associated with $\mathbf{K}_2$. Such finite-size magnetic domains (having up-up-down-down spin structure) instead of true LRO at AFM ordering (T_N) have been predicted for the well-known multiferroic compound Ca_3CoMnO_6, in which the small ferroelectric polarization (compared to that of the theoretically calculated value) is considered to be due to cancellations of polarization originating from different magnetic domains [40]. The occurrence of small ferroelectric polarization for our tilted compound below T_{N2} (see Ref. [25]) may be justified using the same rationale if the ferroelectricity stems from the up-up-down-down spin structure.

In summary, we have revisited magnetic properties of the multiferroic compound $Ba_3HoRu_2O_9$ via comprehensive neutron powder diffraction measurements. We find that this material undergoes two magnetic phase transitions at $T_{N1} \approx 50$ K and $T_{N2} \approx 10$ K, where both Ho and Ru spins develop long-range order simultaneously. This suggests a strong $4d$(Ru)-$4f$ (Ho) magnetic correlation. In addition, below T_{N2} we unravel the coexistence of two magnetic phases associated with two completely different propagation wave vectors, implying a competition among different exchange interactions. The exchange striction from up-up-down-down structure may be the reason for the observation of polarization below T_{N2}. This study demonstrates that the $Ba_3RRu_2O_9$ system provides a unique platform to study the cooperative $4d$-$4f$ phenomena where Ru and R moments are strongly coupled and compete with other exchange interactions. Our results call for a reinvestigation of magnetic orderings in other R-Ru-based systems in general.

Work at Michigan State University was supported by the U.S. Department of Energy, Office of Science, Office of Basic Energy Sciences, Materials Sciences and Engineering Division under Award No. DE-SC0019259.

[1] Y. Tokura, S. Seki, and N. Nagaosa, Rep. Prog. Phys. **77**, 076501 (2014).
[2] S. H. Kang, H. J. Lee, I. W. Kim, T. H. Jang, Y. H. Jeong, and T. Y. Koo, J. Kor. Phys. Soc. **51**, 669 (2007).
[3] N. Hur, S. Park, P. A. Sharma, J. S. Ahn, S. Guha, and S.-W. Cheong, Nature (London) **429**, 392 (2004).
[4] K. Singh, T. Basu, S. Chowki, N. Mahapotra, K. K. Iyer, P. L. Paulose, and E. V. Sampathkumaran, Phys. Rev. B **88**, 094438 (2013).
[5] E. García-Matres, J. L. Martínez, and J. Rodríguez-Carvajal, Eur. Phys. J. B **24**, 59 (2001).
[6] J. G. Rau, E. K.-H. Lee, and H.-Y. Kee, Annu. Rev. Condens. Matter Phys. **7**, 195 (2016).
[7] J. T. Rijssenbeek, P. Matl, B. Batlogg, N. P. Ong, and R. J. Cava, Phys. Rev. B **58**, 10315 (1998).
[8] N. Taira, M. Wakeshima, and Y. Hinatsu, J. Phys.: Condens. Matter **11**, 6983 (1999).
[9] C. R. Wiebe, J. S. Gardner, S.-J. Kim, G. M. Luke, A. S. Wills, B. D. Gaulin, J. E. Greedan, I. Swainson, Y. Qiu, and C. Y. Jones, Phys. Rev. Lett. **93**, 076403 (2004).
[10] S. T. Ku, D. Kumar, M. R. Lees, W.-T. Lee, R. Aldus, A. Studer, P. Imperia, S. Asai, T. Masuda, S. W. Chen, J. M. Chen, and L. J. Chang, J. Phys.: Condens. Matter **30**, 155601 (2018).
[11] N. Taira, M. Wakeshima, Y. Hinatsu, A. Tobo, and K. Ohoyama, J. Solid State Chem. **176**, 165 (2003).
[12] J. S. Gardner and G. Ehlers, J. Phys.: Condens. Matter **21**, 436004 (2009).
[13] X. A. Velásquez Moya, R. Cardona, J. I. Villa Hernández, D. A. Landínez Téllez, and J. Roa-Rojas, J. Electron. Mater. **47**, 3421 (2018).
[14] Y. Hinatsu, Y. Izumiyama, Y. Doi, A. Alemi, M. Wakeshima, A. Nakamura, and Y. Morii, J. Solid State Chem. **177**, 38 (2004).
[15] Y. Izumiyama, Y. Doi, M. Wakeshima, Y. Hinatsu, K. Oikawa, Y. Shimojo, and Y. Morii, J. Mater. Chem. **10**, 2364 (2000).
[16] Y. Shimoda, Y. Doi, M. Wakeshima, and Y. Hinatsu, J. Solid State Chem. **183**, 33 (2010).
[17] Y. Doi, M. Wakeshima, Y. Hinatsu, A. Tobo, K. Ohoyama, and Y. Yamaguchi, J. Mater. Chem. **11**, 3135 (2001).
[18] Y. Doi and Y. Hinatsu, J. Solid State Chem. **177**, 3239 (2004).
[19] W. Miller, M. Avdeev, Q. Zhou, A. J. Studer, B. J. Kennedy, G. J. Kearley, and C. D. Ling, Phys. Rev. B **84**, 220406(R) (2011).
[20] M. S. Senn, S. A. J. Kimber, A. M. Arevalo Lopez, A. H. Hill, and J. P. Attfield, Phys. Rev. B **87**, 134402 (2013).
[21] T. Susuki, N. Kurita, T. Tanaka, H. Nojiri, A. Matsuo, K. Kindo, and H. Tanaka, Phys. Rev. Lett. **110**, 267201 (2013).

[22] H. D. Zhou, E. S. Choi, G. Li, L. Balicas, C. R. Wiebe, Y. Qiu, J. R. D. Copley, and J. S. Gardner, Phys. Rev. Lett. **106**, 147204 (2011).
[23] S. A. J. Kimber, M. S. Senn, S. Fratini, H. Wu, A. H. Hill, P. Manuel, J. P. Attfield, D. N. Argyriou, and P. F. Henry, Phys. Rev. Lett. **108**, 217205 (2012).
[24] J. Hwang, E. S. Choi, F. Ye, C. R. Dela Cruz, Y. Xin, H. D. Zhou, and P. Schlottmann, Phys. Rev. Lett. **109**, 257205 (2012).
[25] T. Basu, V. Caignaert, S. Ghara, X. Ke, A. Pautrat, S. Krohns, A. Loidl, and B. Raveau, Phys. Rev. Mater. **3**, 114401 (2019).
[26] C. D. Ling, Z. Huang, B. J. Kennedy, S. Rols, M. R. Johnson, M. Zbiri, S. A. J. Kimber, J. Hudspeth, D. T. Adroja, K. C. Rule, M. Avdeev, and P. E. R. Blanchard, Phys. Rev. B **94**, 174401 (2016).
[27] T. Basu, A. Pautrat, V. Hardy, A. Loidl, and S. Krohns, Appl. Phys. Lett. **113**, 042902 (2018).
[28] Y. Doi, Y. Hinatsu, Y. Shimojo, and Y. Ishii, J. Solid State Chem. **161**, 113 (2001).
[29] Y. Doi and Y. Hinatsu, J. Mater. Chem. **12**, 1792 (2002).
[30] J. Rodríguez-Carvajal, Physica B **192**, 55 (1993).
[31] A. S. Wills, Physica B **276–278**, 680 (2000).
[32] See Supplemental Material at http://link.aps.org/supplemental/10.1103/PhysRevB.102.020409 for details on the structural and magnetic analysis, detailed figures of magnetization and heat capacity, and Rietveld refinement and magnetic structure at 1.5 K.
[33] B. Prévost, N. Gauthier, V. Y. Pomjakushin, B. Delley, H. C. Walker, M. Kenzelmann, and A. D. Bianchi, Phys. Rev. B **98**, 144428 (2018).
[34] Y. Zhao, J. W. Lynn, G. S. Thakur, Z. Haque, L. C. Gupta, and A. K. Ganguli, J. Phys. Chem. Solids **111**, 1 (2017).
[35] J. Rodríguez-Carvajal and J. Villain, C. R. Phys. **20**, 770 (2019).
[36] S. H. Bukhari, T. Kain, M. Schiebl, A. Shuvaev, A. Pimenov, A. M. Kuzmenko, X. Wang, S.-W. Cheong, J. Ahmad, and A. Pimenov, Phys. Rev. B **94**, 174446 (2016).
[37] N. Hur, S. Park, P. A. Sharma, S. Guha, and S.-W. Cheong, Phys. Rev. Lett. **93**, 107207 (2004).
[38] S. Chattopadhyay, V. Balédent, F. Damay, A. Gukasov, E. Moshopoulou, P. Auban-Senzier, C. Pasquier, G. André, F. Porcher, E. Elkaim, C. Doubrovsky, M. Greenblatt, and P. Foury-Leylekian, Phys. Rev. B **93**, 104406(R) (2016).
[39] X. Ke, J. Peng, W. Tian, T. Hong, M. Zhu, and Z. Q. Mao, Phys. Rev. B **89**, 220407(R) (2014).
[40] Y. J. Choi, H. T. Yi, S. Lee, Q. Huang, V. Kiryukhin, and S.-W. Cheong, Phys. Rev. Lett. **100**, 047601 (2008).